International Journal of Science and Engineering Applications
Volume 12-Issue 09, 144 - 155, 2023, ISSN:- 2319 - 7560
DOI:10.7753/IJSEA1209.1046

Analyzing the Explosive Behavior of a Buckling Restrained Brace Frame Made of Shape Memory Alloy by Using Finite Element Method

Arman Sadeghipour
Department of Civil Engineering
K.N Toosi University of Technology
Tehran, Iran

Reza Khorramabadi
Department of Mechanical Engineering
Ferdowsi University
Mashhad, Iran

Abstract: In this study, we investigate the behavior of a buckling restrained brace frame made of a shape memory alloy when subjected to explosive loads. To accomplish this, we initially loaded a conventional braced frame with a span of 6 meters and a height of 3 meters with explosive forces. The simulation and validation processes will be conducted using the ABAQUS software. After validating the results, we examine eight additional models using ABAQUS software. These models are divided into four groups. In each group, the first sample is constructed from plain steel alloy, while the second sample is made from a shape memory alloy with identical specifications to the first sample. In the first group, the explosive load is set at 10 kilograms, in the second group, it is 30 kilograms, in the third group, it is 50 kilograms, and in the final group, the mass of the explosive material is 100 kilograms. The analysis results reveal that as the amount of explosive material increases, displacement and stress in the samples rise. The displacement increases significantly in the last set of samples (with 100 kilograms of explosive material). By incorporating shape memory alloy into the samples, especially with lower quantities of explosive material, it is possible to partially restore the structure to its initial state, thereby reducing the severity of damage inflicted upon it. Even with higher amounts of explosive material, a substantial level of restoration can be achieved, further minimizing structural damage.

Keywords: Buckling Restrained Brace Frame (BRBF), Shape Memory Alloy, Explosive loading, FEA, Abaqus

1. INTRODUCTION

In various incidents worldwide, the occurrence of attacks on critical structures has led to a special focus on explosive loads in recent years. Understanding the proper behavior of structural systems against lateral loads such as earthquakes, explosive forces, etc., can assist us in designing structures more effectively. Buckling restrained braces (BRBs) are one of the most common lateral load-resisting systems, and their major weakness is related to the buckling of the compressive member, resulting in a reduction in load-carrying capacity. Using non-buckling BRBs is one of the solutions to address this issue. To withstand lateral forces on structures over the past years, various solutions, such as shear walls, converging and diverging braces, and more, have been introduced. As mentioned, due to a significant flaw in bracing systems that involve buckling under compressive loads, further studies were conducted to address this issue, particularly focusing on alleviating compressive buckling phenomena. In addition, design flaws, and uncertain behavior of braces after seismic and explosive events, led to further research and the development of a new type of BRB known as buckling restrained brace frames or BRBFs.

Buckling restrained brace frames consist of a slender steel core to resist axial loads and their ductile behavior with high stability is ensured by the yielding section. Despite the higher impact resilience of isotropic materials like steel alloys, composite materials demonstrate superior strength when subjected to tension or compression loading. Notably, concrete, while categorized as a brittle material, displays heightened resistance to buckling when contrasted with various other composite materials, such as bone [1-2]. A continuous concrete jacket surrounds the steel core to prevent its buckling under compressive forces. A small gap, approximately a few millimeters (typically between 1 to 5 millimeters), separates the steel core and the jacket to prevent force transfer between them, effectively preventing buckling of the metal core during cyclic loading. There are various types of buckling restrained brace technologies based on different configurations of the steel core and concrete-filled jacket to achieve high performance in these braces. One of them is buckling restrained braces with a concrete-filled steel jacket, while another is all-steel buckling restrained braces [3]. These days the most important factor in designing the structures is their stability under the loads. To address this issue some researchers are working on different ways and methods to increase the reliability of structures under the loads. For instance, Mohammad Ali et al [4] This research investigates the buckling behavior of elliptical CDFST columns using transverse reinforcements in the outer tube. The study simulates an elliptical column and is subjected to compressive loading using Abaqus Software. The results show an increase in load-bearing capacity with the highest compressive strength in columns using transverse reinforcements, which enhance the stability of columns under loads. Nazeryan and Feizbahr simulated the seismic performance of Composite reinforced concrete and steel (RCS) joints under cyclic and uniform loads using ABAQUS finite element software. A modified model was presented, increasing capacity, and exhibiting more stable behavior, enhancing the system's appeal [5]. Ferdosi and Porbashiri investigated the material properties of carbon nanotubes to use them as a composite to reinforce the structures. They employed the novelty method called the asymptotic homogenization method [6].

Buckling restrained braces, despite their excellent resistance to buckling, suffer from issues such as deformations and residual strains after earthquake loading [7]. Various solutions to mitigate this weakness have been proposed in different studies, including geometric reshaping, sandwiching, the use of composite materials, and more. One of the approaches that has been recently employed to restore materials to their

International Journal of Science and Engineering Applications
Volume 12-Issue 09, 144 - 155, 2023, ISSN:- 2319 - 7560
DOI:10.7753/IJSEA1209.1046

original state after plastic deformation is the use of smart materials that can return to their initial state after undergoing plastic deformation. Therefore, considering the need for significant deformations that occur during explosive loading in structures and the requirement for returning to the original state in buckling restrained braces, this research focuses on the application of smart materials in buckling restrained braces using ABAQUS software. The impact of using these materials in braces and the degree of return to the initial state after explosive loading will be investigated.

At a large and macroscopic scale, superelastic shape memory materials exhibit a hysteresis behavior similar to the diagram below. This hysteresis curve indicates the restoration of the original shape and the energy dissipation properties of these materials. Total axial strains of more than 1 to 3 percent and a significant portion of axial strains with values greater than 3 percent have the capability to return (Figure 1). The presence of these unique properties in shape memory materials has led to the diversification of their applications in various fields over the past two decades [8-12]. In addition, as Zadeh et al. [13] conclude, investigating concrete recycling within the construction industry is imperative, as the industry faces historical environmental challenges. It must adapt and adopt sustainable practices to mitigate its impact on the environment and address concerns related to resource depletion, waste generation, and global warming. The incorporation of the 3R principles of reduce, reuse, and recycle presents a potent means to curtail waste generation in the construction industry, with a particular focus on addressing concrete and demolition waste, given concrete's widespread use in construction. Furthermore, the adoption of life cycle design principles not only underscores the significance of recycling but also promotes the establishment of a closed-loop system, synergistically contributing to fostering a more sustainable construction industry and effectively addressing the complexities posed by environmental and resource-related concerns.

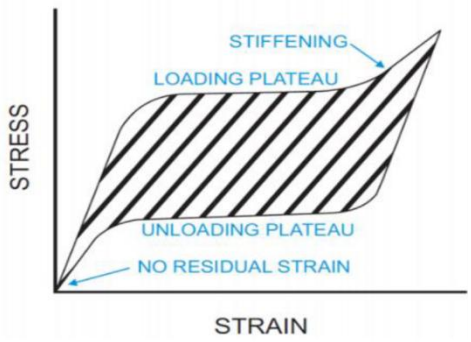

Figure 1. Ideal Stress-Strain Behavior of Superelastic Shape Memory Alloy [9]

Buckling restrained braces (BRBs), which were first used in Japan in 1989, are now widely employed worldwide as flexible, earthquake-resistant components in earthquake-prone regions such as Japan, the United States, Taiwan, China, Turkey, and New Zealand [14]. Alborzi et al. [15], conducted a numerical comparison of the impact of conventional and composite buckling restrained braces on seismic protection of short and mid-rise steel buildings. They stated that buckling restrained braces are a specific type of bracing system that exhibits acceptable behavior in energy dissipation without buckling under compressive forces. However, the presence of residual deformations during strong ground motions in these braces is significant, arising from the low post-yield stiffness in these systems. New systems, referred to as composite buckling restrained braces, offer better performance against seismic loads, and in this research, these systems will be compared alongside conventional systems. Feng et al. [16], focused on designing damage control in buckling restrained braces using masonry walls based on the displacement response spectrum in the elastic region. They aimed to investigate the seismic design and performance of buckling restrained braces using masonry walls. They also mentioned that the reason for using masonry walls is to reduce drift in frames equipped with buckling restrained braces. Fayeq et al. [17] investigated the seismic performance of frames with buckling restrained braces with changes in beam-to-column connections. Kiggins et al. [18] examined residual drift in frames with buckling restrained braces as a dual system. They stated that frames with buckling restrained braces exhibit very good behavior in energy dissipation. However, the low post-yield stiffness in these braces results in significant drift in the structure. Wan and Choi [19] focused on seismic design, nonlinear analysis, and performance assessment of frames with buckling restrained braces. They mentioned that buckling restrained braces have been widely used in high seismic regions recently, attributed to their unique features compared to converging braces. Matthew et al. [20] investigated earthquake collapse prevention in new buckling restrained braces using the ASCR41 code. Mahmoudi and Zaree [21] evaluated displacement enhancement factors in frames with converging and buckling restrained braces. Chung and Chen [22] conducted tests and finite element analysis on sandwich buckling restrained braces. They proposed a new type of buckling restrained braces and conducted tests and finite element analysis on them. From the study done by (Khanal, 2020; Khanal et al., 2023), a numerical analogy can be performed on implementing nonlinear one-dimensional and three-dimensional buckling equations in the material behavior using the software MATLAB and ANSYS APDL. This analogy technique helps to validate the real buckling behavior using a numerical approach [23-24]. Zhao et al. [25] examined corner frictional connections to enhance the seismic performance of buckling restrained braces through a subset of tests. Wanga et al. [26] investigated the collapse capacity of reinforced concrete bridges strengthened with buckling restrained braces. They focused on bridges' collapse capacity and failure modes strengthened with buckling restrained braces in columns. Esfandiari and Soleimani [27] conducted laboratory tests on buckling restrained braces with an optimized one percent of polypropylene and composite fibers in their microstructure under seismic loads. Vaismoradi et al. [28] evaluated the collapse risk of frames with buckling restrained braces during earthquakes and their aftershocks. Jia et al. [29] examined the experimental and cyclic behavior of composite frames with buckling restrained braces.

2. RESEARCH METHOD

This research is divided into two parts, simulating the application of shape memory alloys. The first part involves validating the results based on a reference paper [30]. Initially, a single-span, single-story frame with specifications from this reference paper is simulated, and the simulation process is validated using ABAQUS software. In the second step, the main models of this research, consisting of 8 models with similar specifications to the validation case, are simulated in ABAQUS software. The explosive load values are varied among 10-, 30-, 50-, and 100-kilograms equivalent to TNT explosive material. These models are analyzed in both

International Journal of Science and Engineering Applications
Volume 12-Issue 09, 144 - 155, 2023, ISSN:- 2319 - 7560
DOI:10.7753/IJSEA1209.1046

simple frames and frames with shape memory alloys, and the results are extracted and compared. The details of these models are presented in Table 1 within this article.

Table 1. Specifications of the analyzed samples in this paper [30].

Model	Name	Amount of explosive charge TNT (kg)
Validation model	-	Explosive-induced compressive load in accordance with the reference paper.
Model No.1	plain steel	10
Model No.2	Shape Memory Alloy	10
Model No.3	plain steel	30
Model No.4	Shape Memory Alloy	30
Model No.5	plain steel	50
Model No.6	Shape Memory Alloy	50
Model No.7	plain steel	100
Model No.8	Shape Memory Alloy	100

2.1 Simulation Geometry

The geometry of the buckling restrained brace frame is extracted from the reference paper [30] and is consistent for all 8 other models analyzed in this research. For this purpose, a single-span frame with a buckling restrained brace under explosive loading is modeled in the ABAQUS software. This frame has a height of 3 meters and a span length of 6 meters, incorporating a buckling restrained brace. The frame consists of two columns and one beam on top, connected to the structure by a series of brace stiffeners. The beam used in the analysis is of type W1835, and the columns are of type W1468. The geometry of the beam and column used in the analyzed structure is presented in Figure 2.

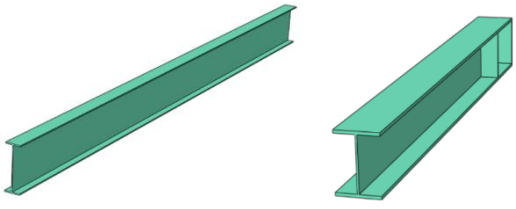

Figure 2. Geometry of the beam and column used in the validation analysis and other models of the paper. (Beam on the left, column on the right)

The beam and column used in the analysis are of the W type, and the cross-sectional parameters and specifications for the beam and column are presented in Figure 3 and Table 2, respectively.

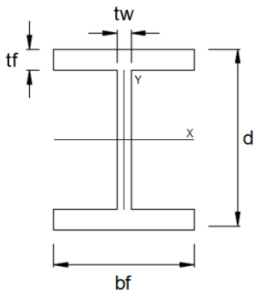

Figure 3. Cross-Sectional Parameters of the Beam and Column Used in the Validation Model [30].

The next component used in the modeling is the buckling restrained brace (BRB), which consists of a steel core and a concrete cover. The specifications and dimensions of the core and cover are presented in Figure 4.

Table 2. Parameters Used for the Cross-Section of the Beam and Column [30].

Type	*tf*	*tw*	*bf*	*d*
Beam	10.8	7.6	152.4	449.6
Column	18.3	10.5	254.9	356.6

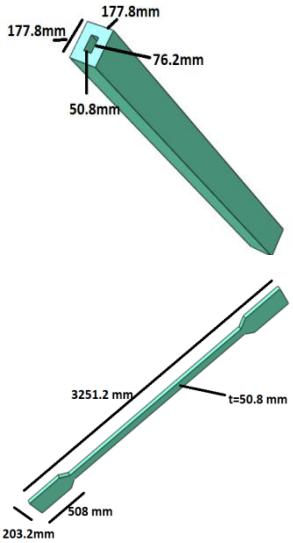

Figure 4. The geometry of the steel core and concrete cover of the buckling restrained brace used in the models.

The steel used for the beams and columns in the validation models and models with regular steel is A992, while the steel used for other sections of the models is A36. Additionally, the concrete used for the cover of the buckling restrained braces has a density of 2400 kilograms per cubic meter and a maximum compressive strength of 31 MPa. These material properties were defined using the CDP model. The elastic and plastic properties of these steels are presented in Table 3.

International Journal of Science and Engineering Applications
Volume 12-Issue 09, 144 - 155, 2023, ISSN:- 2319 - 7560
DOI:10.7753/IJSEA1209.1046

Table 3. Properties of steels used in the validation section [30].

Type of steel	A992	A36
Ultimate Tensile Strength (MPa)	448	399
Yield Strength (MPa)	344	248
Poisson's ration	0.3	0.3
Young's Modulus (MPa)	200	200
Density (Kg/m^3)	7850	7850

Superelastic properties have been used in the ABAQUS software for simulating shape memory alloy materials employed in the nuclear steel moment frame section. This feature in the material library of the software allows for accurate simulation of these materials. Shape-memory materials possess superelastic properties, which means their elastic region is much broader than that of common materials like steel. Typically, steel undergoes plastic deformation at strains exceeding one percent, whereas superelastic materials can have elastic deformations of up to 8 percent. The general stress-strain behavior of superelastic materials is presented in Figure 5.

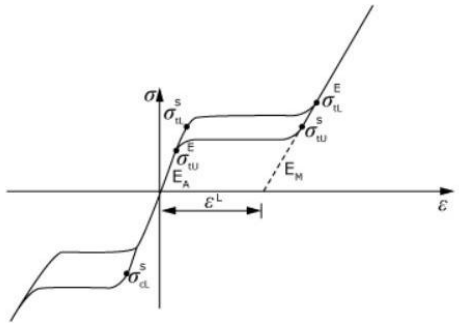

Figure 5. Stress-Strain Curve of Superelastic or Shape-Memory Materials [31].

In this figure, A represents the austenite phase, and M represents the martensite phase. As observed in the figure, for defining smart materials in general within the ABAQUS software, you need the elastic modulus of austenite and martensite, the Poisson's ratio of austenite and martensite, the transformation strain, loading and unloading stress points on the first and second slopes. These properties for a superelastic material have been extracted from the reference article [31], and these coefficients are presented in Table 4.

Table 4. Required Properties for Simulating shape memory alloy Materials [31].

Young's Modulus of Martensite (GPa)	50
Young's Modulus of Austenite (GPa)	37
Poisson's Ratio	0.35
Transformation Strain L (%) ε	5.5
Martensitic Transformation Starting Stress (MPa)	400
Martensitic Transformation Ending Stress (MPa)	650
Austenitic Transformation Starting Stress (MPa)	350
Austenitic Transformation Ending Stress (MPa)	80

2.2 Assembly of the Validation Model

After defining the material properties in the previous section, in this section, the model has been assembled based on the specifications outlined in the reference article. The assembly model is presented in Figure 6. This assembly geometry remains consistent for all models in this article, with variations only in the explosive load and the type of materials in the central core of the moment-resisting frames.

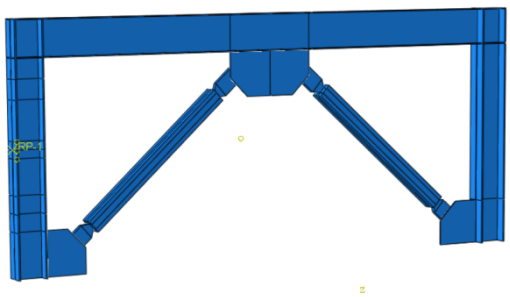

Figure 6. Assembly Model for the Validation Sample.

2.3 Constraints for the Validation Model

The connection of beams to columns has been achieved using coupling constraints. Additionally, to ensure the model's integrity, constraints such as tie constraints have been utilized for connecting the moment-resisting frame to the strengthening plates, the central core section, the concrete cover, and other parts of the model. For this purpose, as shown in Figure 7, coupling constraints have been selected for the beam-to-column connections. The regions where tie constraints have been applied are also presented in Figures 8 to 10.

International Journal of Science and Engineering Applications
Volume 12-Issue 09, 144 - 155, 2023, ISSN:- 2319 - 7560
DOI:10.7753/IJSEA1209.1046

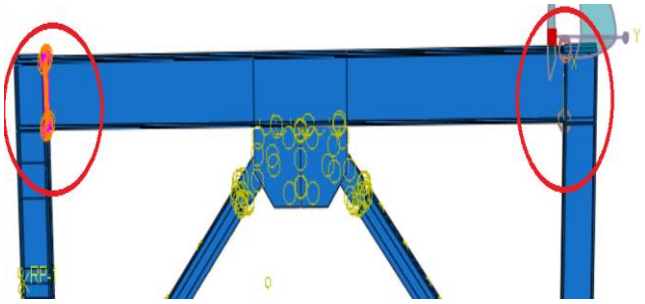

Figure 7. Beam-to-Column Connection with Coupling Constraint.

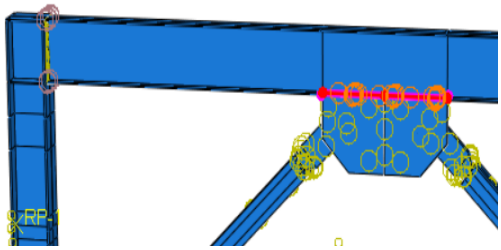

Figure 8. Connection of Central Reinforcer to the Central Beam with Tie Constraint.

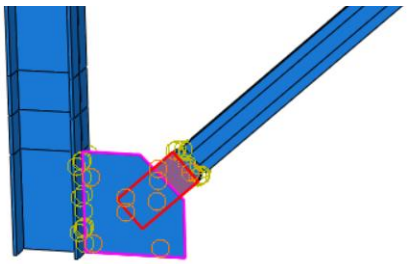

Figure 9. Connection of Reinforcer to the Moment-Resisting Frame with Tie Constraint.

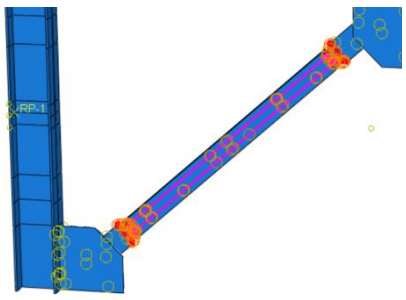

Figure 10. Connection of Steel Central Core and Concrete Cover of the Buckling-Restrained Moment Frame with Tie Constraint.

2.4 Loading and Boundary Conditions

Since the lower portions of the structure are connected to the ground, all degrees of freedom for the lower parts of the structure are constrained, as shown in Figure 11. These boundary conditions remain consistent for both the validation model and the other models in this article.

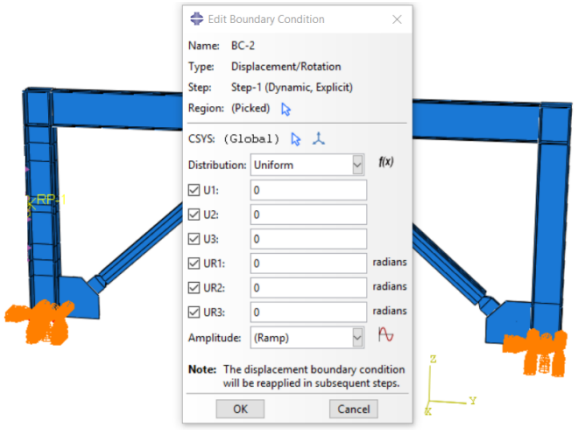

Figure 11. Constrained Lower Portions of the Validation Model.

After constraining the lower portions of the structure, the explosive load must be applied to the structure. Following the proposed approach in the reference article [30], the explosive load is applied as an extremely high-pressure load over a very short duration, as illustrated in Figure 12, to the left side of the structure as depicted in Figure 13. The pressure load increases linearly from zero to its maximum value of 58 bars over a duration of 22 milliseconds. In the other models in this article (Models 1 to 8), the explosive load is applied to the structure at a distance of 3 meters from the structure using the Conweb property in the ABAQUS software, following the pattern shown in Figure 12, with values of 10, 30, 50, and 100 kilograms of TNT.

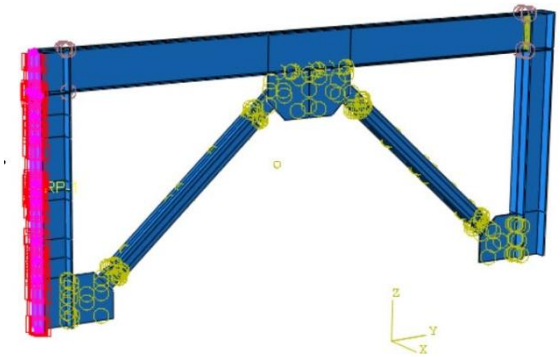

Figure 12. Explosion Initiation Point and Initial Impact Area of the Blast Wave with the Structure.

2.5 Meshing of Models

For analysis, the models are meshed with a 2-centimeter discretization, and the C3D8R element type is used for meshing. The C3D8R element is a 3D 8-node element capable of modeling various types of nonlinear behaviors resulting from the explosion. The meshed model is presented in Figure 13.

International Journal of Science and Engineering Applications
Volume 12-Issue 09, 144 - 155, 2023, ISSN:- 2319 - 7560
DOI:10.7753/IJSEA1209.1046

Figure 13. Meshed Model for the Validation Model.

3. DISCUSSION AND RESULTS

The results related to the validation model and other results obtained from the analysis of the 8 simulated models in this section will be presented. First, the results of the validation model will be provided, followed by the results of the analyzed models.

3.1 Results Related to the Validation Model

In this section, the results related to the validation model will be presented. The validation model, as previously described, was a single-span frame with a height of 3 meters and a span of 6 meters, equipped with a buckling-restrained moment frame and subjected to explosive loading. The explosive load was applied as a 58-bar pressure load over a duration of 22 milliseconds to the left side of the structure. The maximum displacement of the left side of the structure under this loading was extracted from ABAQUS software, and it is compared with the results presented in the reference article [30] in Figure 14.

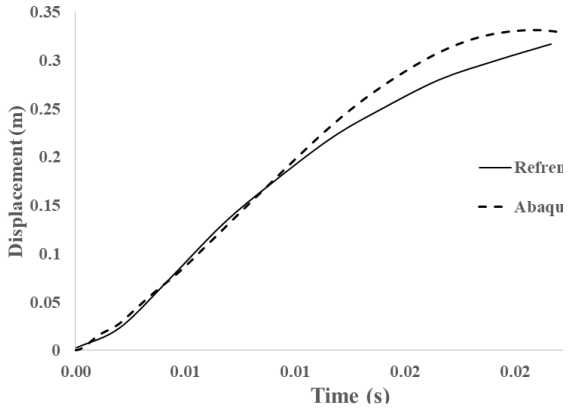

Figure 14. Comparison of the Displacement of the Left Column of the Model with the Results Presented in Reference [30].

As observed in Figure 14, the displacement of the left column in the analyzed model closely aligns with the displacement of the sample presented in reference [30]. Any slight discrepancies can be attributed to meshing errors and considering that the difference between the two samples is less than 5 percent, the results are considered **acceptable** with good accuracy.

3-2. Presentation of results related to Model No.1 (plain steel with 10-kilogram TNT).

In this model, as indicated in its title, the amount of explosive material was 10 kilograms, and the blast distance was 3 meters. The stress and displacement graph for this sample is presented in Figure 15.

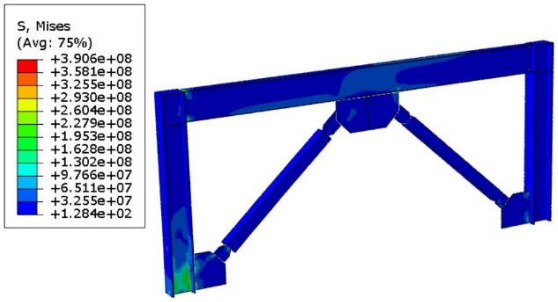

(a)

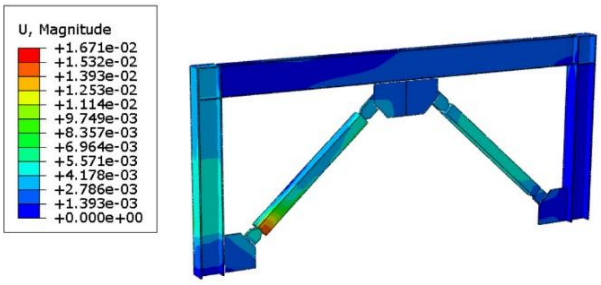

(b)

Figure 15. Displacement and Stress in Model No.1 (a) Stress, (b) displacement.

As shown in Figure 15, the explosive loading resulting from a 10-kilogram TNT explosion has had a significant impact on the structure. Although the maximum stress in the structure is approximately 390 MPa, most areas are in the blue region, indicating that they experienced lower stress levels. Only the support region of the left column is shown in green, where stress levels range from 260 to 290 MPa in the structure. In this region, even plain steel is expected to return to its initial state and undergo minimal deformation since the stress is below the yield strength of the steel material.

The maximum displacement in the structure occurs in the concrete shell section, measuring 16 millimeters. In the steel sections of the structure, the maximum displacement is 8 millimeters at the end of the analysis. The reason for not returning to the initial state after loading in the system can be attributed to the failure of the concrete shell and the impossibility of returning to the initial state in the bracing elements due to the interaction between the steel and concrete components.

International Journal of Science and Engineering Applications
Volume 12-Issue 09, 144 - 155, 2023, ISSN:- 2319 - 7560
DOI:10.7753/IJSEA1209.1046

3-3. Presentation of Results in Model No.2 (Shape Memory Alloy with 10-Kilogram TNT)

In this section, conditions like model No.2 were applied to the structure, with the only difference being the use of a smart alloy instead of plain steel. The stress and displacement contour plot in the structure is presented in Figure 16.

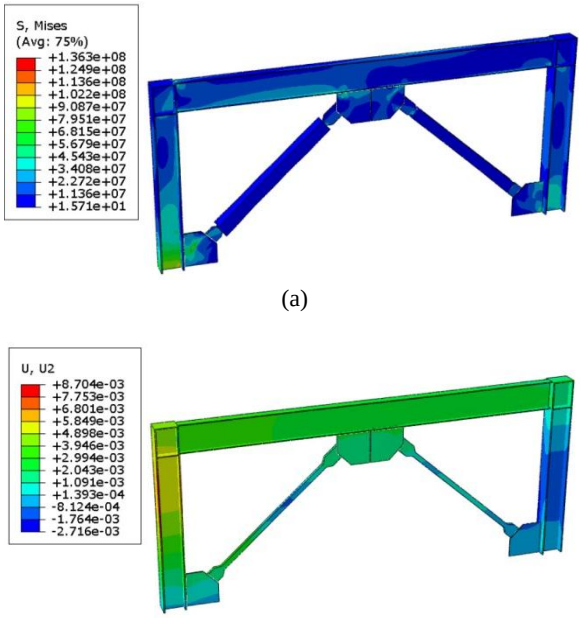

Figure 16. Displacement and Stress in Model No.2 (a) Stress, (b) displacement.

As shown in Figure 16, the maximum stress in the structure at the end of the analysis is 136 MPa, which is much lower compared to the regular sample. This means that the structure has been able to recover itself, reducing the final stresses in the component. The displacement value in the sample at the end of the analysis is 7.8 millimeters, which is equal to the displacement in model No.1, which was without shape memory alloys. The reason for this is that the explosive load couldn't push the structure into the plastic deformation zone, and it remained within the elastic range. Therefore, in both models, the displacement value at the end of the analysis is almost equal. However, it is expected that with an increase in the explosive load in other models, the difference between these two models will become more pronounced.

3-4. Presentation of Results in Model No.3 (Plain Steel with 30-Kilogram TNT)

In this section, the results related to model No.3 are presented. In this model, ordinary steel with the properties of the steel model for validation has been used throughout the structure, and an explosive load of 30 kilograms at a distance of 3 meters from the structure has been applied. The stress and displacement contour in this model is presented in Figure 17.

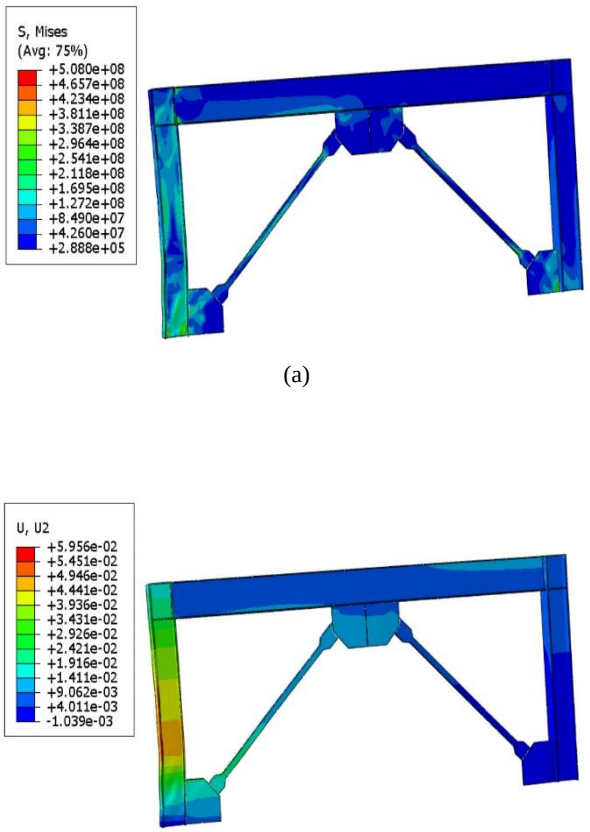

Figure 17. Displacement and Stress in Model No.3 (a) Stress, (b) displacement.

As seen in Figure 17, the maximum stress in the model has exceeded the plastic limit and reached a value of 508 MPa. With this stress, it is expected that the structure undergoes more deformation compared to model number 1. Continuing with the contour plot of displacement in model number 3, as observed in the figure, the displacement in the structure, as expected, has increased compared to model number 1 and reached 59 millimeters. The structure was unable to recover itself and entered the plastic region, and this deformation in the structure has remained permanent.

3-5. Presentation of Results in Model No.4 (Shape Memory Alloy with 30-Kilogram TNT)

In this section, the results related to the sample containing a shape memory alloy with a 30-kilogram explosive material will be presented. In this sample, all conditions are identical to Sample No.4, with the only difference being the use of a shape memory alloy instead of plain steel. The results for stress and displacement contour plots in this sample are presented in Figure 18.

International Journal of Science and Engineering Applications
Volume 12-Issue 09, 144 - 155, 2023, ISSN:- 2319 - 7560
DOI:10.7753/IJSEA1209.1046

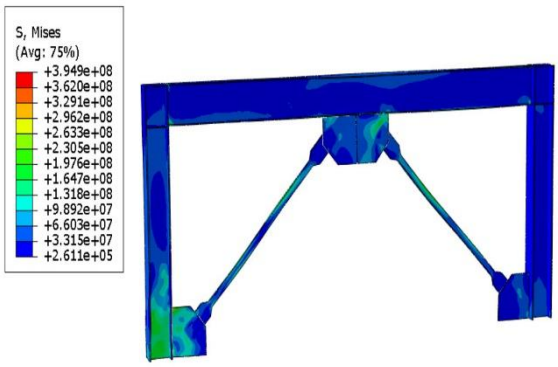

(a)

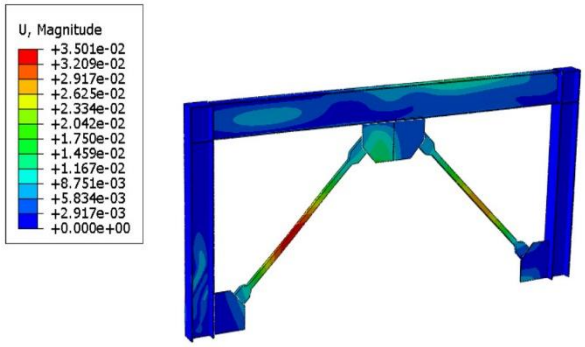

(b)

Figure 18. Displacement and Stress in Model No.4 (a) Stress, (b) displacement.

In Figure 18, the highest stress value in the structure is within the green region and is approximately 270 MPa. The stress value of 394 MPa is attributed to modeling error. As seen, the structure, compared to model No. 3, has been able to recover itself to a significant extent. The small remaining stress in the structure is due to non-recovery in regions involving supports and concrete shells in the moment-resisting frames. Overall, the structure has been able to recover almost 70% of its initial state. As shown in the figure (displacement contour), the structure has returned to its initial state in areas other than the moment-resisting frames. Only in the central areas of the moment-resisting frames, where the frame contacts the concrete section, the structure has not fully recovered due to concrete damage and interaction between these two parts of the structure. However, compared to the simple state, it has recovered significantly, with the displacement reducing from 60 millimeters to 35 millimeters in those areas.

3-6. Presentation of Results for Model No. 5 (Plain Steel with 50-Kilogram TNT)

In this section, the results related to model No. 5 are presented. In this model, the explosive load has increased to 50 kilograms, and plain steel has been used for the metallic components. The contour plots for displacement and stress distribution in this model are shown in Figure 19.

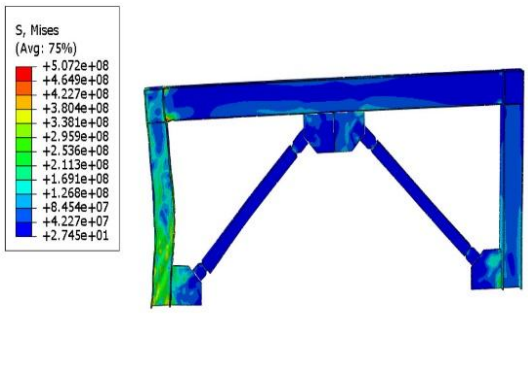

(a)

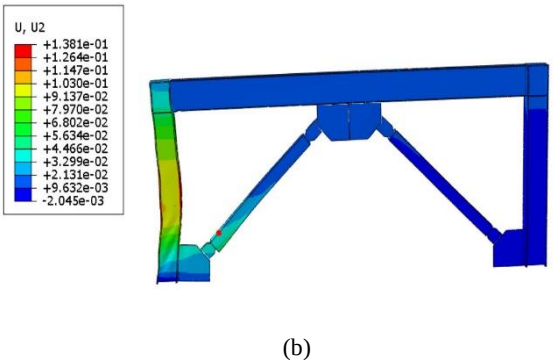

(b)

Figure 19. Displacement and Stress in Model No.5 (a) Stress, (b) displacement.

As observed in Figure 19, the highest stress value in the structure is approximately 507 MPa, and it is in the regions where the beam is connected to the column. In this sample, the stress level has exceeded the elastic limit, and high-stress regions in the structure have increased. It is expected that permanent displacement in the structure will increase.

The distribution of displacement in model No.5, at the end of the analysis, is equal to 138 millimeters, which is 2.5 times higher compared to Model No. 3. This indicates that with an increase in the mass of the explosive material, the displacement in the structure will increase nonlinearly.

3-7. Presentation of Results for Model No. 6 (Shape Memory Alloy with 50-Kilogram TNT)

In this section, the results related to model No. 5 are presented. In this model, the explosive load has increased to 50 kilograms, and plain steel has been used for the metallic components. The contour plots for displacement and stress distribution in this model are shown in Figure 19.

International Journal of Science and Engineering Applications
Volume 12-Issue 09, 144 - 155, 2023, ISSN:- 2319 - 7560
DOI:10.7753/IJSEA1209.1046

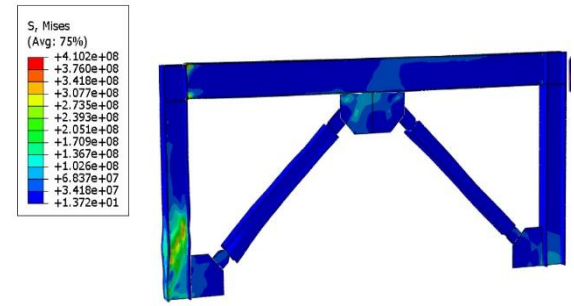

(a)

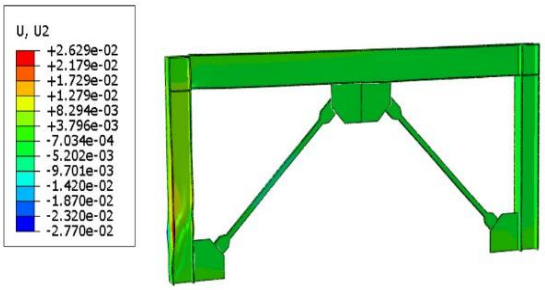

(b)

Figure 20. Displacement and Stress Distribution in Model No.6 (a) Stress, (b) displacement.

As observed in Figure 20, the stress value in this sample is approximately 410 MPa. This stress has significantly decreased in the connection regions, and the model has been able to recover itself, reducing the stress level compared to the sample with plain steel.

Continuing with the contour plot of displacement distribution in the structure, the maximum displacement value in model No.6 is 26 millimeters, which is a significant improvement compared to model No.5, where it was 138 millimeters. In this case, the structure has almost fully recovered itself, except in the regions where stress was high and slight buckling occurred due to column bending.

3-8. Presentation of Results for Model No.7 (Plain Steel with 100-Kilogram TNT)

In this sample, the mass of the explosive material has increased to 100 kilograms. With this increase, it is expected that both stress and displacement in the sample will significantly increase. The stress contour plot in this sample is presented in Figure 21.

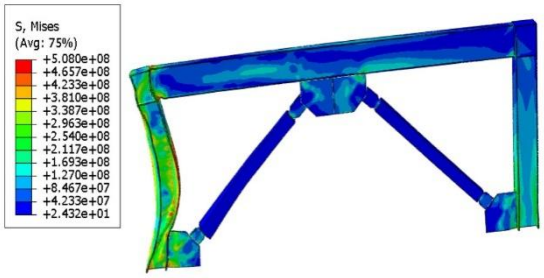

(a)

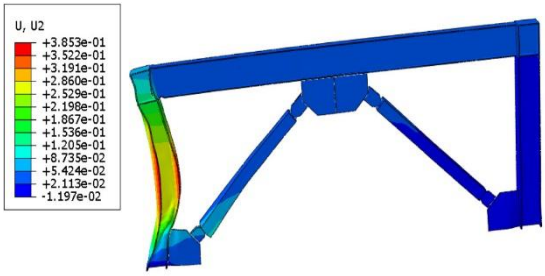

(b)

Figure 21. Displacement and Stress Distribution in Model No.7 (a) Stress, (b) displacement.

As shown in Figure 21, the deformation in the structure is very significant, and high-stress areas have increased. Almost the column on the left side is directly exposed to the explosive load, and the structure has undergone buckling. The maximum displacement in the structure in this model is 385 millimeters, which is a severe displacement and has caused significant bending in the left-side column. If there were no bracing in the system, the structure would have experienced a complete collapse. The results obtained indicate severe damage to the structure under high explosive loads.

3-9. Presentation of Results for Model No.8 (Shape Memory Alloy with 100-Kilogram TNT)

In this section, the results related to model No.8 are presented. In this model, all the conditions are like model No.7, with the only difference being the use of shape memory alloy instead of plain steel in the model. The distribution of displacement and stress in this model is presented in Figure 22.

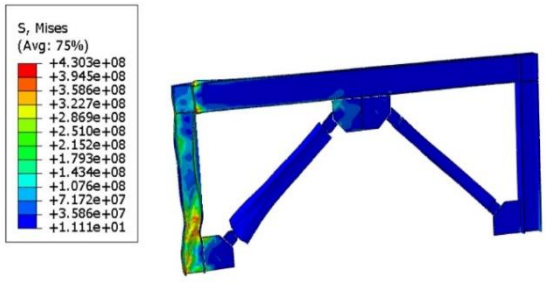

International Journal of Science and Engineering Applications
Volume 12-Issue 09, 144 - 155, 2023, ISSN:- 2319 - 7560
DOI:10.7753/IJSEA1209.1046

(a)

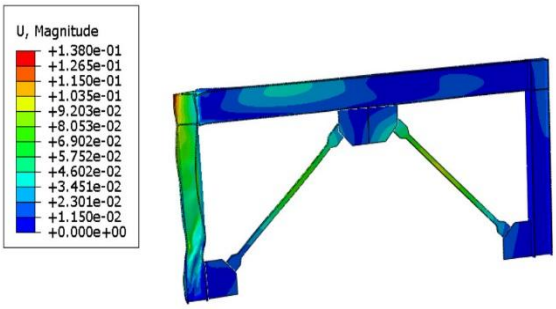

(b)

Figure 22. Displacement and Stress Distribution in Model No.8 (a) Stress, (b) displacement.

As illustrated in Figure 22, the stress levels in the structure have decreased compared to model No.7, which used plain steel. High-stress areas in the structure have also significantly reduced. In other words, the model has managed to recover itself to some extent and get closer to its initial form.

According to Figure 22, although the explosive load on the structure was very high, and deformations were significant, the structure has been able to recover itself to a large extent. The displacement has decreased from 385 to 138. The reason for not returning to the initial state can be attributed to the bending of columns and interaction with supports and the concrete shell, which has prevented a complete return. However, to a considerable extent, this severe deformation has been reduced.

To summary the obtained results, table 5 is presented. As illustrated on table 5, because of using shape memory alloy material on beams and columns, the applied stress decreased 55, 22, and 19 percent for 10, 30 and 50 kg TNT, respectively. Moreover, deformation dropped to less than half for all of the models. Finally, in model 7, the column of the structure buckled and collapsed due to the explosion, resulting in a displacement of 385 millimeters. In contrast, model 8, which utilized shape memory alloy, reduced the displacement to 138 millimeters, but it couldn't fully recover.

Table 5. The comparison of results for plain steel and shape memory alloy by using FEA.

Model	Name	Amount of explosive charge TNT (kg)	Stress (MPa)	Deformation (mm)
Validation model	-	Explosive-induced compressive load in accordance with the reference paper.	-	-
Model No.1	plain steel	10	290	16
Model No.2	Shape Memory Alloy	10	136	8.7
Model No.3	plain steel	30	508	59
Model No.4	Shape Memory Alloy	30	394	35
Model No.5	plain steel	50	507	138
Model No.6	Shape Memory Alloy	50	410	26
Model No.7	plain steel	100	Collapse	385
Model No.8	Shape Memory Alloy	100	-	138

4. CONCLUSION

This research focuses on investigating the behavior of a moment-resisting frame equipped with shape memory alloy under explosive loads. Initially, a single-span, single-story moment-resisting frame with a 3-meter span and 6-meter height, as described in reference [30], was selected. It was subjected to explosive loading with a pressure load generated by an explosion of 58 times the explosive charge within 22 milliseconds. The maximum displacement on the left side of the structure was extracted and compared with the reference paper's results for validation.

Following validation, eight additional models were analyzed. In all eight models, including the geometry and support conditions, the modeling approach was similar to the validation model. Among these eight models, four had properties similar to the validation model, using ordinary steel, while the other four models used shape memory alloy in

the core of the moment-resisting frame. These eight models were exposed to explosive loads of 10, 30, 50, and 100 kilograms, categorized in pairs.

In the first category, which included models 1 and 2, the explosive load was 10 kilograms. The structure in model 1 did not enter the plastic region and returned to its original state to a significant extent due to its elastic properties. In model 2, which used shape memory alloy, the recovery was even greater. The displacement in both models at the end of the analysis was 8 millimeters, but the stress in model 2 decreased from 290 MPa in model 1 to 138 MPa due to the use of shape memory alloy material.

In the second category, models 3 and 4 were exposed to a 30-kilogram explosive load. The displacement in model 3 at the end of the analysis was 60 millimeters, whereas it was reduced to 35 millimeters in model 4. Additionally, the stress values decreased from 508 to 394 MPa when shape memory alloy material was used.

In the third category, models 5 and 6 were subjected to a 50-kilogram explosive load. The displacement at the end of the analysis for these two models was 138 and 26 millimeters, respectively, and the stress decreased from 507 to 410 MPa, demonstrating the structure's recovery using shape memory alloy.

In the last category, models 7 and 8 faced a 100-kilogram explosive load from an explosive material. In model 7, the column of the structure buckled and collapsed due to the explosion, resulting in a displacement of 385 millimeters. In contrast, model 8, which utilized shape memory alloy, reduced the displacement to 138 millimeters, but it couldn't fully recover.

In conclusion, the findings of this research indicate that the use of shape memory alloy in structures can significantly mitigate the damage caused by explosive loads and restore structures that have undergone substantial deformations to their original state.

REFERENCES

[1] Moradi, H., Rafi, R., & Muslim, A. (2021). Crack growth simulation in 13th row of compressor blades under foreign object damage and resonant vibration condition. *Journal of Vibroengineering*, *23*(1), 44-62.

[2] Moradi, H., Beh Aein, R., & Youssef, G. (2021). Multi-objective design optimization of dental implant geometrical parameters. *International Journal for Numerical Methods in Biomedical Engineering*, *37*(9), e3511.

[3] Weng Y T, Lin J L, Tsai C Y and Tsai K C. (2005). Analytical assessment of a 2-story BRBF for full-scale 3D sub-structural pseudo-dynamic testing. The First Conference on Advanced in Experimental Structural Engineering (AESE), Nagoya, Japan.

[4] Mohammed Ali, A., Besharat Ferdosi, S., Kareem Obeas, L., Khalid Ghalib, A., & Porbashiri, M. (2024). Numerical study of the effect of transverse reinforcement on compressive strength and load-bearing capacity of elliptical CFDST columns. *Journal of Rehabilitation in Civil Engineering*, *12*(1).

[5] Akbari, A., Nikookar, M., & Feizbahr, M. (2013). Reviewing Performance of Piled Raft and Pile Group Foundations under the Earthquake Loads. *Research in Civil and Environmental Engineering*, *1*(5), 287-299.

[6] S. B. Ferdosi, M. Porbashiri, (2022). Calculation of the Single-Walled Carbon Nanotubes' Elastic Modulus by Using the Asymptotic Homogenization Method, International Journal of Science and Engineering Applications 11, 254–265.

[7] Nazeryan, M., & Feizbahr, (2022). M. Seismic Evaluation of the Cheng and Chen Modified Model Using Shear Keys in Steel Beam-to-Concrete Column Connections.

[8] Dolce M, & Cardone D. (2001). Mechanical behaviour of shape memory alloys for seismic applications. Martensite, and austenite NiTi bars subjected to torsion. International Journal of Mechanical Sciences, 43(11), 2631-2656.

[9] Han Y L. (2003). Structural Vibration Control by Shape Memory Alloy Damper. Earthquake engineering & structural dynamics, 32:(3), 483-94.

[10] Hu J W. (2013). Numerical Simulation for the Behavior of Superelastic Shape Memory Alloys. Journal of Mechanical Science and Technology, 27(2): 381-86.

[11] Omar M. (2014). Seismic Response of Braced Steel Frames with Shape Memory Alloy and Mega Bracing Systems. World Academy of Science, Engineering and Technology, International Journal of Civil, Environmental, Structural, Construction and Architectural Engineering, 8:(2), 131-38.

[12] Zadeh, S. S., Joushideh, N., Bahrami, B., & Niyafard, S. (2023). A review on concrete recycling.

[13] Tabrizi, H. (2023). Evaluation of the Effect of Vegetation on Free Surface Flow Behavior, COMPUTATIONAL RESEARCH PROGRESS IN APPLIED SCIENCE & ENGINEERING, Vol. 9, Issue. 1, 1-5.

[14] Wada E, Saeki T Takeuch and A Watanabe. (1989). Development of unbounded brace. Column Technical Publication, Vol. 12, no. 115.

[15] M Alborzi M H, Tahghighi M H, Azarbakh A. (2019). Numerical comparison on the efficiency of conventional and hybrid buckling restrained braces for seismic protection of short-to-mid-rise steel buildings. International Journal of Advanced Structural Engineering.

[16] Yulong Feng, Zhi Zhang, Xun Chong, JingWu, Shaoping Meng. (2018). Elastic displacement spectrum-based design of damage-controlling BRBFs with rocking walls. Journal of Constructional Steel Research 148, 691–706.

[17] Ahmad Fayeq Ghowsi and Dipti Ranjan Sahoo. (2013). Seismic Performance of Buckling-restrained Braced Frames with Varying Beam-column Connections. International Journal of Steel Structures, Vol 13, No 4, 607-621.

[18] Shawn Kiggins, Chia-Ming Uang. (2006). Reducing residual drift of buckling-restrained braced frames as a dual System, Engineering Structures 28, 1525–1532.

[19] Jong-Wan Hu and Eunsoo Choi. (2014). Seismic Design, Nonlinear Analysis, and Performance Evaluation of Recentering Buckling-restrained Braced Frames (BRBFs). International Journal of Steel Structures, Vol 14, No 4, 683-695.

[20] Matthew S, Speicher J L, Harris III. (2018). Collapse Prevention seismic performance assessment of new bucklingrestrained braced frames using ASCE 41. Engineering Structures 164, 274–289.

[21] Mussa Mahmoudi and Mahdi Zaree. (2013). Evaluating the displacement amplification factors of concentrically braced steel frames. International Journal of Advanced Structural Engineering, 5:13.

[22] Chung-Che Choua, Sheng-Yang Chen. (2010). Subassemblage tests and finite element analyses of sandwiched buckling-restrained braces. Engineering Structures 32, 2108-2121.

[23] Khanal, M., Zhou, J., & Fan, X. (2023). Analytical Solution for Moisture Diffusion with Initial Non-Uniform Moisture Concentration used in Bake Time Study in Electronics Packaging. *2023 24th International Conference on Thermal, Mechanical and Multi-Physics Simulation and Experiments in Microelectronics and Microsystems (EuroSimE)*, 1–7. https://doi.org/10.1109/EuroSimE56861.2023.10100783

[24] Khanal, M. (2020). *Baking Schedule for Moisture-Sensitive Electronic Packages* [M.E.S., Lamar University Beaumont]. https://www.proquest.com/docview/2452513196/abstract/C5362DD0FB914165PQ/1.

[25] Junxian Zhao, Ruobing Chen, Zhan Wang, Yi Pan. (2018). Sliding corner gusset connections for improved buckling-restrained braced steel frame seismic performance: Subassemblage tests. Engineering Structures 172, 644–662.

[26] Yuandong Wanga, Luis Ibarra, Chris Pantelides. (2019). Collapse capacity of reinforced concrete skewed bridges retrofitted with buckling-restrained braces. Engineering Structures 184, 99–114.

[27] Esfandiari J, Soleimani E. (2018). Laboratory investigation on the buckling restrained braces with an optimal percentage of microstructure. polypropylene and hybrid fibers under cyclic loads, Composite Structures, 203, 585–598.

[28] Veismoradi S, Cheraghi A, Darvishan E. Probabilistic mainshock-aftershock collapse risk assessment of buckling restrained braced frames. Soil Dynamics and Earthquake Engineering 115 (2018) 205–216.

[29] Mingming Jia, Dagang Lu, Lanhui Guo, Lin Sun. (2014). Experimental research and cyclic behavior of buckling-restrained braced composite frame. Journal of Constructional Steel Research 95, 90–105.

[30] Charco, O. Effects of blast loading on buckling-restrained braces of a single-and two-bay chevron frame. Master of science in structural engineering, California state university, Northridge, 2018.

[31] Nuno Rebelo, Xiao-Yan Gong, Amy Hall, Alan R Pelton and Tom W Duerig. (2004). Finite Element Analysis on the Cyclic Properties of Superelastic Nitinol, ABAQUS Users' Conference.